Quantum-defect and distorted-wave theory applied to the resonance contribution of inelastic electron scattering

R. E. H. Clark, A. L. Merts, J. B. Mann, and L. A. Collins
Los Alamos National Laboratory, Los Alamos, New Mexico 87545
(Received 18 October 1982)

The importance of the resonance contributions to inelastic scattering of electrons from atoms and ions has been appreciated for quite some time. We have used an approximate method to compute the resonance contributions to selected inelastic transitions in O VI and S IV and compare our results with other theoretical calculations. We find that our total resonance-enhanced collision strengths are in very good agreement with other calculations. We also can accurately compute the positions of individual resonances but can sometimes be in error by a factor of 2 on individual resonance widths.

I. INTRODUCTION

The presence of closed channels in the S matrix for electron scattering from atomic systems can give rise to resonance structure in the computed cross section. Some early estimates[1] using the Green's function for the Coulomb field indicated that the average resonance contribution may be very large compared to the background cross section. Other investigations have been carried out using distorted-wave techniques directly,[2,3] close-coupling techniques,[4] close coupling along with quantum-defect theory,[5,6] distorted wave with quantum-defect theory,[7,8] and perturbation theory.[9] In the present paper we use close-coupling, distorted-wave, and Coulomb-Born calculations coupled with quantum-defect theory on O VI and compare these results to those of Bhadra and Henry[6] and Presnyakov and Urnov.[1] In order to estimate how well the method works for less highly charged ions, we have carried out distorted-wave calculations coupled with quantum defect on the $^2P^o$-$^4P^e$ transition in S IV and compare our results with Dufton and Kingston.[4]

II. METHOD

A. Positions and Widths of the Resonance

The use of quantum-defect theory for determining the positions and widths of resonances has been formulated by Seaton.[10] We briefly summarize his formulation here using his notation. He forms the matrix $\underline{\chi}$ from the reactance matrix $\underline{R}$

$$\underline{\chi}=(i-\underline{R})(i+\underline{R})^{-1} . \tag{1}$$

The $\underline{R}$ matrix is usually slowly varying with energy and is thus fitted by a low-order polynomial in energy. Thus the $\underline{\chi}$ matrix can be computed at any energy from the fit parameters for the $\underline{R}$ matrix. A matrix $\underline{\zeta}$ is then formed from the $\underline{\chi}$ matrix. $\underline{\zeta}$ is formed such that it differs only by a phase factor from the $\underline{S}$ matrix for open channels. Thus the collision strength for an inelastic transition between two open channels can be given in terms of $\underline{\zeta}_{oo}$, the submatrix of $\underline{\zeta}$ corresponding to open channels. Seaton gives $\underline{\zeta}_{oo}$ in terms of $\underline{\chi}$,

$$\underline{\zeta}_{oo}=\underline{\chi}_{oo}-\underline{\chi}_{oc}(\underline{\chi}_{cc}-e^{-2\pi i\nu_c})^{-1}\underline{\chi}_{co} , \tag{2}$$

where a subscript o refers to open and c refers to closed. Thus, for example, $\underline{\chi}_{co}$ is the submatrix of $\underline{\chi}$ connecting closed and open channels. The ν_c is a complex effective quantum number for channel c. The energy can be written in terms of ν_c

$$E=E_c-\frac{Z^2}{\nu_c^2} , \tag{3}$$

where E_c is the energy of channel c and Z is the residual charge.

One sees that at certain (complex) values of the energy, $\underline{\zeta}_{oo}$ given by Eq. (2) will have poles. These poles will give rise to resonances in the collision strength. These resonances will form a Rydberg-like series. To see this we write ν_c in terms of an integer n and a complex quantum defect μ_c:

$$\nu_c=n-\mu_c(E) . \tag{4}$$

The quantum defect in general is relatively slowly varying with energy. Thus, if a resonance occurs at an initial value of ν_c it will be repeated whenever ν_c changes by an integer.

We can associate a pole energy with the closed channel giving rise to the pole through the quantum defect. As noted previously, the reactance matrix is

 ©1983 The American Physical Society

slowly varying with energy. Also, for a diagonal reactance matrix, the relation

$$R_{ii}=\tan\delta_i \tag{5}$$

holds where δ_i is the phase shift. We use this relation as an approximation for the nondiagonal $\underline{R}$ matrix. The quantum defect is then related to the analytic continuation of the phase shift by

$$\mu_i=\frac{1}{\pi}\delta_i \tag{6}$$

(see Seaton[11]). We thus obtain a first approximation to the quantum defect for each closed channel by fitting the reactance matrix above threshold, extrapolating below threshold, and using Eqs. (5) and (6). Picking a value of n for use in Eq. (4), we obtain an approximate pole position from Eq. (3). As discussed below, the exact pole position can be found to very good precision by numerical methods. One can then use this value of E and the value of E_c for the closed channel corresponding to the R_{ii} used to find ν_c. Use of Eq. (4) then gives the complex quantum defect.

Writing the complex quantum defect as

$$\mu=\alpha+i\beta\,, \tag{7}$$

the resonance series will occur at energies

$$E_r=E_c-\frac{Z^2}{(n-\alpha)^2}\,, \tag{8}$$

where E_c is the threshold energy of the closed channel and will have widths of

$$\Gamma_r=\frac{4Z^2(n-\alpha)\beta}{[(n-\alpha)^2+\beta^2]^2}\,, \tag{9}$$

as given by Norcross and Seaton.[5] Thus one sees that finding the widths and positions of the resonances is equivalent to finding the poles of $\underline{\zeta}_{oo}$ which is equivalent to finding the zeros of the determinant

$$|\underline{\chi}_{cc}-e^{-2\pi i\nu_c}|=0\,. \tag{10}$$

For the case in which all the closed channels have the same threshold energy, the poles can be found by a diagonalization of $\underline{\chi}_{cc}$.[10] In the cases we consider here, the closed channels have different threshold energies. We have determined the roots of Eq. (10) and thus the quantum defects by numerical procedures.

A straightforward method for finding the zeros of the determinant given by Eq. (10) is to evaluate the determinant at three distinct energy points and fit it to a quadratic. This then predicts a closer approximation to the zero. This process is iterated. Some care must be taken that the original three energy points are closely spaced relative to the separation between successive resonances in a Rydberg series corresponding to different values of n in Eq. (8). This method has proven satisfactory, providing good pole positions in less than ten iterations in most cases. The value of the quantum defect was found to usually be slowly varying with energy so that it is a good predictor of positions and widths along a Rydberg series.

A second numerical approach to the solution of Eq. (10) was to find the eigenvalues of $\underline{\chi}_{cc}-e^{-2\pi i\nu_c}$. If the eigenvalue is zero, then the determinant is zero. The zero eigenvalue was found by perturbation theory. This method gave agreement with the method outlined above.

The computer program RANAL[12] was written to implement many of the procedures outlined above. A preliminary version of RANAL was provided by Christensen.[13] We modified the program so that the degenerate closed-channel method of Seaton could be used. We had noted that the perturbation theory of Cowan[9] has worked well in other cases and that his method does not include channel coupling. We thus modified RANAL so that it could be made to ignore all but one set of degenerate closed channels so that the formulation of Seaton[10] was applicable. This method produced results that were in excellent agreement with the results from the numerical procedures outlined above.

B. Collision strengths

For the case of degenerate closed channels one can use Seaton's[10] formulation to obtain a Gailitis[14]-type

TABLE I. Collision strengths in O VI at 5.9 Ry computed by different methods with $L\leq 4$.

	2s-2p	2s-3s	2p-3s
DW[a] GA[d]	1.68	0.281	0.787
CC[b] GA	1.61	0.271	0.848
Hyd[c] GA	1.22	0.266	0.655
DW DCC[e]	1.63	0.340	0.921
CC DCC	1.57	0.316	0.905
Hyd DCC	1.24	0.235	0.549
DW AV[f]	1.63	0.333	0.810
CC AV	1.67	0.310	0.834

[a]DW, distorted wave.
[b]CC, close coupling.
[c]Hyd, Coulomb-Born calculation with hydrogenic bound-state wave functions.
[d]GA, Gailitis average of original RANAL program.
[e]DCC, Using one set of degenerate closed channels at a time in RANAL.
[f]AV, simple numerical average of detailed collision strength.

TABLE II. Comparison of the GA and AV collision strength using close-coupling matrix elements above threshold for the O VI case at 5.9 Ry.

	2s-2p		2s-3s		2p-3s	
Symmetry	GA[a]	AV[b]	GA	AV	GA	AV
^1S	0.082	0.085	0.015	0.013	0.044	0.021
^3S	0.128	0.128	0.002	0.002	0.007	0.003
^1P	0.134	0.135	0.029	0.028	0.137	0.114
^3P	0.133	0.130	0.046	0.051	0.081	0.086
^1D	0.032	0.012	0.067	0.075	0.113	0.084
^3D	0.003	0.003	0.033	0.032	0.066	0.058
^1F	0.223	0.222	0.025	0.025	0.129	0.193
^3F	0.118	0.118	0.027	0.027	0.038	0.035
^1G	0.324	0.302	0.019	0.051	0.149	0.161
^3G	0.436	0.436	0.008	0.007	0.085	0.078
Total	1.61	1.67	0.271	0.310	0.848	0.834

[a]GA, Gailitis average of original RANAL program.
[b]AV, simple numerical average of detailed collision strength.

average collision strength. In practice it appears that this method gives acceptable results when the difference in the threshold energies is small relative to the energy difference between the lowest closed channel and the energy point at which the collision strength is being computed. In cases where the degenerate theory does not apply, we have used two alternative methods.

One method is a simple numerical average. The detailed collision strength can be calculated from the $\underline{\zeta}_{oo}$ matrix of Eq. (2). This matrix can be obtained from the fit coefficients for the reactance matrix and thus does not require very much computer time. In fact, $\underline{\zeta}_{00}$ and, hence, the collision strength, can be computed thousands of times in seconds of CPU (central processing unit) time on a large computer such as a Contral Data Corporation CDC-7600. Thus the numerical average can be made quite accurate by using a suitably fine energy mesh.

Our second approach to the collision strength was to use the Gailitis average limited to one set of degenerate closed channels at a time. We obtain the final result as a sum of the resonance enhancements and the background contribution. This method gave collision strengths which agreed very well with the numerical averaging procedure.

III. RESULTS

A. O VI

For O VI we have comparisons of results from a number of combinations of computational methods. We have calculated the reactance matrix above threshold by close-coupling, distorted-wave,[15] and Coulomb-Born hydrogenic approximations. The close-coupling calculation used the linear algebraic approach based on the integral equation formulation of Collins and Schneider[16,17] and included the 2s, 2p, 3s, 3p, and 3d states. The different reactance matrices were extrapolated below some of the thresholds with the use of RANAL to obtain the resonance-enhanced collision strengths. We computed the enhanced collision strength by the original RANAL program, the simple numerical average, and by using sets of degenerate closed channels. We carried out these calculations at 5.9 Ry, which is above the 3s threshold at 5.82 Ry but below the 3p (6.06 Ry) and 3d (6.13 Ry) thresholds. We present here our calculated collision strengths for the 2s-2p, 2s-3s, and 2p-3s transitions. These calculations were carried out to total system L of 4 since most of the resonance contributions come from the lower-lying angular momentum states. In Table I we show the total collision strengths computed by the different

TABLE III. Comparison of collision strengths in O IV at 5.9 Ry.

Method	$\Omega(2s,3s)$	$\Omega(2p,3s)$
CC[a] GA[d]	0.362	1.19
DW[b] GA	0.372	1.13
Hyd[c] GA	0.347	0.93
Bhadra and Henry[e]	0.38	1.2
Presnyakov and Urnov[f]	0.43	3.9

[a]CC, closed-coupling reactance matrix above threshold.
[b]DW, distorted-wave reactance matrix above threshold.
[c]Hyd, Coulomb-Born with hydrogenic target wave functions above threshold.
[d]GA, Gailitis-type average.
[e]Reference 6.
[f]Reference 1.

combinations of methods. One sees that the difference in the methods is not exceedingly large. For this case we note that the energy of 5.9 Ry is 0.16 Ry below the $3p$ threshold and that the $3d$ threshold is only 0.07 Ry above the $3p$ threshold. Thus the approximation that all the closed channels have the same threshold energy is not far off. In Table II we compare collision strengths for each symmetry calculated by the Gailitis average method versus the simple numerical average when the above threshold matrix elements were computed from the close-coupling approximation. One sees that in some cases the partial-wave values differ by a large amount but that the totals agree quite well.

We also compare our total collision strengths with other theoretical results in Table III. Our total collision strengths include the resonance-enhanced collision strengths out to $L=4$, and the background collision strengths for higher-L values. The Bhadra and Henry[6] results were estimated from their graphs. One sees that our distorted-wave and close-coupling results are both in very good agreement with them and that our Coulomb-Born hydrogenic results are not in serious disagreement. To obtain the Presnyakov and Urnov[1] collision strengths we normalized their background cross sections to our background collision strengths of 0.18 for the $2s$-$3s$ and 0.13 for the $2p$-$3s$ transitions at an energy of 6.2 Ry. We then used these normalization factors to obtain their collision strengths at 5.9 Ry. We note that this normalization to the close-coupling background gives collision strengths somewhat larger than our hydrogenic background, but not by a substantial amount. We see that with this normalization, the Presnyakov and Urnov result for the $2s$-$3s$ transition agrees well with the other results. However, the $2p$-$3s$ result is in serious disagreement. We are confident that the source of the disagreement is not in the use of hydrogenic wave functions, since our hydrogenic results are in good agreement with the more elaborate methods. We do note that there appears to be a problem in the vertical scale of the $2p$-$3s$ graph of Presnyakov and Urnov. Specifically, the label of 150 on that graph appears to be placed at a position corresponding to about 600 on the logarithmic scale. Thus, we are unsure of the actual value of the cross section for the $2p$-$3s$ transition obtained by Presnyakov and Urnov.

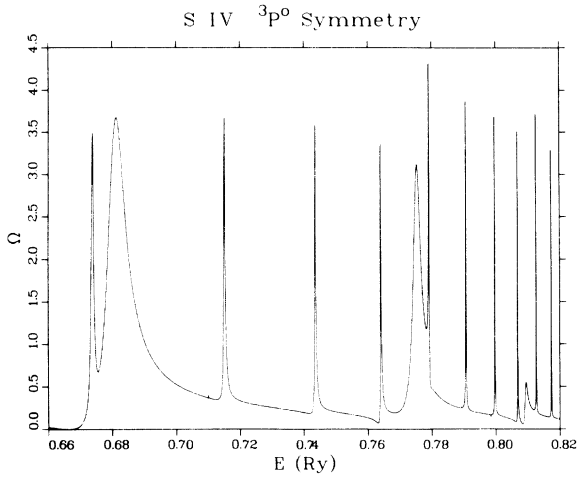

FIG. 2. Collision strength vs energy showing the presence of resonances in the $3s^23p\ ^2P$-$3s3p^2\ ^4P$ transition, $^3P^o$ symmetry, in S IV.

B. S IV

We consider next the $3s^23p(^2P)$-$3s\,3p^2(^4P)$ transition in S IV. We chose this case because we wanted

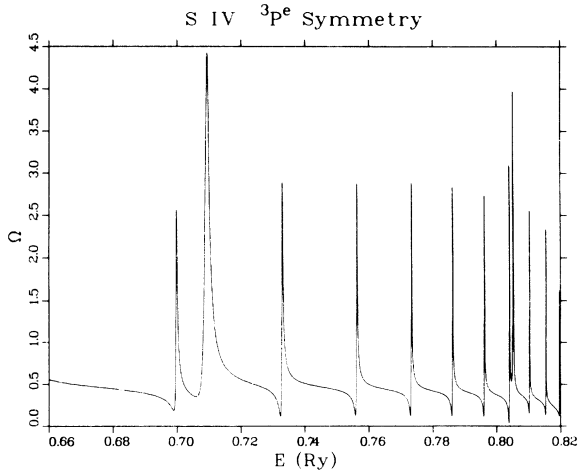

FIG. 1. Collision strength vs energy showing the presence of resonances in the $3s^23p\ ^2P$-$3s3p^2\ ^4P$ transition, $^3P^e$ symmtery, in S IV.

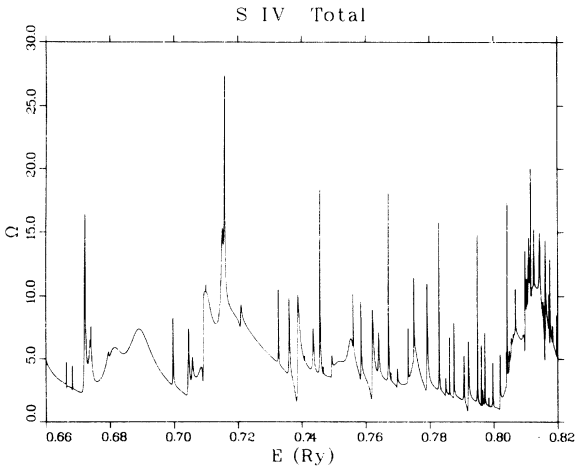

FIG. 3. Total collision strength vs energy showing the presence of resonances in the $3s^23p\ ^2P$-$3s3p^2\ ^4P$ transition in S IV.

TABLE IV. Target-state mixtures used.

Dominant configuration	Configurations included	Mixing coefficient
$3s^23p\ ^2P$	$3s^23p(^2P)$	0.975 37
	$3p^3(^2P)$	0.164 47
	$3s3p(^1P)3d(^2P)$	0.116 71
	$3s3p(^3P)3d(^2P)$	−0.089 29
$3s3p^2\ ^4P$	$3s3p^2(^4P)$	0.995 01
	$3s3d^2(^4P)$	0.072 98
	$3p^2(^3P)3d(^4P)$	0.068 03
$3s3p^2\ ^2D$	$3s3p^2(^2D)$	0.892 34
	$3s^23d(^2D)$	0.422 09
	$3s3d^2(^2D)$	0.053 53
	$3p^2(^3P)3d(^2D)$	0.130 43
	$3p^2(^1S)3d(^2D)$	0.075 38
$3s3p^2\ ^2S$	$3s3p^2(^2S)$	0.985 00
	$3s3d^2(^2S)$	0.172 44
$3s3p^2\ ^2P$	$3s3p^2(^2P)$	0.968 61
	$3s3d^2(^2P)$	0.046 35
	$3p^2(^3P)3d(^2P)$	0.142 23
	$3p^2(^1D)3d(^2P)$	0.198 55
$3s^23d\ ^2D$	$3s^23d(^2D)$	0.880 72
	$3s3p^2(^2D)$	−0.418 64
	$3s3d^2(^2D)$	−0.090 25
	$3p^2(^3P)3d(^2D)$	−0.060 70
	$3p^2(^1D)3d(^2D)$	−0.009 04
	$3p^2(^1S)3d(^2D)$	0.192 77

to try the method on a complex ion with a relatively low level of ionicity. Also, a close-coupling calculation for this transition has been performed by Dufton and Kingston.[4]

We illustrate the effect of resonances on this transition in Figs. 1—3. Figure 1 is a graph of collision strength versus energy for the $^3P^e$ symmetry; Fig. 2 is for the $^3P^o$ symmetry and Fig. 3 is the collision strength summed over the $^3P^o$, $^3P^e$, $^3D^o$, $^3D^e$, $^3F^o$, $^3F^e$, $^3G^o$, and $^3G^e$ symmetries which are all the symmetries included in the calculations done here for this transition. Figures 1 and 2 are included for comparison with Figs. 2 and 3, respectively, of Dufton and Kingston.

In contrast to the O VI case, where mixing effects in the target state are quite small, configuration interaction mixing in S IV is an important effect. However, intermediate-coupling-type mixing has been found to be extremely small and thus has been neglected. The Hartree-Fock target-state mixtures used in the present calculations have been computed using the programs of Cowan[18] and are summarized in Table IV. Note that if one uses the Fano-Racah phase convention in the wave-function definition, the phase for all the minor components (with the exception of the values 0.422 09 and −0.418 64) will be changed.

We have computed the quantum defect by a variety of methods for the $^3P^e$ and $^3P^o$ symmetries and compare them in Tables V and VI. First, we used the modified degenerate closed-channel theory on the distorted-wave resonance matrix calculated above the thresholds both with and without configuration interaction. We also used this theory with the close-coupling reactance matrix of Dufton and Kingston[4] calculated above the thresholds and kindly provided to us by Aggarwal.[19] We note that for these calculations we have used only five or six energy points for the reactance matrix in the region above threshold. Finally, from the positions E_r and widths Γ of the resonances in the Dufton and Kingston paper, we calculated the corresponding values of α and β using Eqs. (8) and (9). In general, we note good agreement on the real part α of the quantum defect. Thus the positions of the resonances should be predicted consistently well by the different methods. The imaginary part β shows more variation. For the most part, the agreement is better than a factor of 2. There are some cases with significantly higher discrepancies. However, these resonance series have been found to be quite weak and add practically nothing to the total collision strength.

We have used the quantum defects calculated from the distorted-wave reactance matrix with configuration interaction to find the positions and widths of the resonances. We compare these with those of Dufton and Kingston for the $^3P^e$ and $^3P^o$

TABLE V. Quantum defects for the $^3P^e$ symmetry in S IV at 0.70 Ry.

Configuration	α^{PNM}[a]	α^{PCI}[b]	α^{DKRM}[c]	α^{DKP}[d]	β^{PNM}	β^{PCI}	β^{DKRM}	β^{DKP}
$3s3p^2(^2D)nd$	0.311	0.309	0.28	0.34	0.010 3	0.006 89	0.010 3	0.0063
$3s3p^2(^2P)ns$	1.206	1.206	1.24	1.24	0.011 7	0.008 41	0.016 8	0.0077
$3s3p^2(^2P)nd$	0.314	0.319	0.43	0.34	0.003 89	0.000 526	0.000 65	0.005
$3s^23d(^2D)nd$	0.340	0.339	0.64	0.26	0.000 612	0.001 96	0.083	0.003

[a]PNM, Present results with no mixing.
[b]PCI, Present results with configuration interaction included.
[c]DKRM, Results from Dufton and Kingston's reactance matrix elements above threshold.
[d]DKP, Results from Dufton and Kingston's (Ref. 4) positions and widths.

TABLE VI. Quantum defects for the $^3P^o$ symmetry in S IV at 0.70 Ry.

Configuration	α^{PNM}[a]	α^{PCI}	α^{DKRM}	α^{DKP}	β^{PNM}	β^{PCI}	β^{DKRM}	β^{DKP}
$3s3p^2(^2D)np$	0.891	0.892	0.936	0.93	0.0122	0.00787	0.00957	0.0088
$3s3p^2(^2D)nf$	1.0362	1.0387	0.952		0.00170	0.0000133	0.00227	
$3s3p^2(^2S)np$	0.892	0.893	0.970	0.99	0.0122	0.0110	0.0225	0.0099
$3s3p^2(^2P)np$	0.892	0.899	0.996	0.98	0.0140	0.0127	0.0174	0.012
$3s^23d(^2D)np$	0.927	0.928	0.924	0.91	0.00149	0.00372	0.00504	0.003
$3s^23d(^2D)nf$	0.0270	0.0273	0.598	0.29	0.00132	0.00137	0.0101	0.011

[a]Abbreviations same as in Table V.

symmetries in Tables VII and VIII. In order to be consistent in the comparison of the resonance positions, we have used the threshold energies of Dufton and Kingston in Eq. (8) in every case. These threshold energies in Rydbergs are 0.61 for the $3s3p^2(^4P)$ state, 0.846 for the $3s3p^2(^2D)$, 1.1514 for the $3s3d^2(^2S)$, 1.2461 for the $3s3p^2(^2P)$, and 1.4304 for the $3s^23d(^2D)$. As noted above, one expects the observed good agreement in the calculated positions of the resonances. Also, because of the variation in β, one sees that the widths show some disagreement. In fact, for the $3s^23d(^2D)nf$ resonances for the $^3P^o$ symmetry, the disagreement is substantial. Thus we caution that the distorted-wave matrix elements coupled with quantum-defect theory should not be used for a detailed analysis of individual resonances. However, it does appear that the method is quite useful in predicting the positions of the resonances and, in most cases of strong resonances, a fair estimate of the width. We note that the quantum defects are very slowly varying with energy and that Tables VII and VIII were made up with values of α and β calculated at 0.70 Ry.

In order to illustrate the effect of the resonances on the average collision strength, we consider the quantity

$$I=\int_{E_L}^{E_u}\Omega(E)dE\ , \tag{11}$$

where $\Omega(E)$ is the detailed collision strength including resonances. We give a graph of I versus energy for the $^3P^o$ symmetry in the energy range 0.66—0.82 Ry in Fig. 4 and from 0.66 to 1.4 Ry in Fig. 5. We use these graphs to illustrate the following points. First, we note that a local value of the collision strength is simply the slope of I. That is,

$$\Omega_{av}=\frac{\int_{E_L}^{E_L+\Delta E}\Omega(E)dE}{\Delta E} \tag{12}$$

TABLE VII. Comparison of positions and widths of resonances to the $^2P^o$-$^4P^e$ transition in S IV for the $^3P^e$ symmetry.

Configuration	E_r^{P}[a](Ry)	E_r^{DK}[b](Ry)	Γ^{P}(Ry)	Γ^{DK}(Ry)
$3s3p^2(^2D)7d$	0.6450	0.6440	0.0008	0.0011
$3s3p^2(^2D)8d$	0.6938	0.6930	0.0005	0.0006
$3s3p^2(^2D)9d$	0.7268	0.7269	0.0004	0.0003
$3s3p^2(^2D)10d$	0.7502	0.7501	0.0003	0.0002
$3s3p^2(^2D)11d$	0.7673	0.7675	0.0002	0.0002
$3s3p^2(^2D)12d$	0.7802	0.7804	0.0002	0.0001
$3s3p^2(^2P)6d$	0.9673	0.9648	0.0001	0.0009
$3s3p^2(^2P)7s$	0.9781	0.9743	0.0016	0.0015
$3s^23d(^2D)5d$	1.0161	1.0327	0.0007	0.0009
$3s3p^2(^2P)8s$	1.0512	1.0490	0.0010	0.0010
$3s3p^2(^2P)9s$	1.0980	1.0967	0.0006	0.0006
$3s3p^2(^2P)10s$	1.1298	1.1278	0.0004	0.0004
$3s^23d(^2D)6d$	1.1496	1.1577	0.0004	0.0007
$3s3p^2(^2P)12s$	1.1690	1.1690	0.0002	0.0002
$3s^23d(^2D)8d$	1.2771	1.2803	0.0002	0.0003
$3s^23d(^2D)9d$	1.3104	1.3126	0.0001	0.0002
$3s^23d(^2D)10d$	1.3340	1.3353	0.0001	0.0001
$3s^23d(^2D)11d$	1.3512	1.3521	0.0001	0.0001

[a]P, Present results.

[b]DK, Results of Dufton and Kingston (Ref. 4).

TABLE VIII. Comparison of positions and widths of resonances to the $^2P^o$-$^4P^e$ transition in S IV for the $^3P^o$ symmetry.

Configuration	$E_r^{P^a}$(Ry)	E_r^{DK}(Ry)	Γ^P(Ry)	Γ^{DK}(Ry)
$3s3p^2(^2D)8p$	0.6679	0.6666	0.0008	0.0009
$3s3p^2(^2P)5p$	0.7110	0.6903	0.0066	0.0053
$3s3p^2(^2D)9p$	0.7092	0.7085	0.0005	0.0006
$3s3p^2(^2D)10p$	0.7376	0.7374	0.0004	0.0005
$3s3p^2(^2S)6p$	0.8064	0.7879	0.0030	0.0023
$3s^23d(^2D)5p$	0.8876	0.8847	0.0020	0.0004
$3s3p^2(^2P)6p$	0.9003	0.8934	0.0034	0.0029
$3s3p^2(^2S)7p$	0.9101	0.9017	0.0017	0.0019
$3s3p^2(^2S)8p$	0.9733	0.9683	0.0011	0.0012
$3s3p^2(^2P)7p$	1.0043	0.9993	0.0020	0.0029
$3s3p^2(^2S)9p$	1.0145	1.0114	0.0007	0.0006
$3s3p^2(^2S)10p$	1.0429	1.0410	0.0005	0.0005
$3s3p^2(^2P)8p$	1.0677	1.0677	0.0013	0.0011
$3s^23d(^2D)6p$	1.0805	1.0815	0.0010	0.0008
$3s^23d(^2D)7p$	1.1863	1.1864	0.0006	0.0007
$3s^23d(^2D)8f$	1.2888	1.2819	0.0001	0.0007
$3s^23d(^2D)9p$	1.2923	1.2928	0.0003	0.0002

[a]Abbreviations same as in Table VII.

gives a locally averaged collision strength. The resonances show up as jumps in I on the graphs. It is seen that the effects of a series of resonances is to increase the average slope of I and to thus increase the average collision strength. In fact, on the detailed graph, Fig. 4, one can esimate the enhancement due to one converging series of resonances by estimating the slope at the right-hand side of the graph. The background collision strength can be estimated from the slope between the jumps near the middle of the graph. We have found numerically that the Gailitis average collision strength computed by the quantum-defect method with the nondegenerate closed channels uncoupled is in agreement with the slope of this graph. One can also define an average collision strength over the entire energy interval as simply the final value of I divided by the total energy range. This value agrees quite well with the sum of the results of the Gailitis average done over all the closed channels separately.

A second point to be made from the graph is that the resonance enhancement to the collision strength and hence to the rate coefficient is a cumulative process. Even narrow resonances can make a significant enhancement. One sees that there is a series of small closely spaced jumps in I in the energy region around 0.80 Ry. Each individual jump is relatively small and comes from a narrow resonance. Howev-

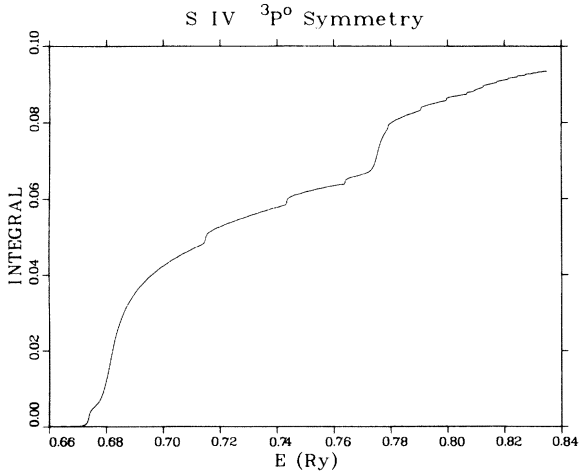

FIG. 4. Plot of the integral of Ω vs energy over the energy region 0.66–0.82 Ry for the $^3P^o$ symmetry.

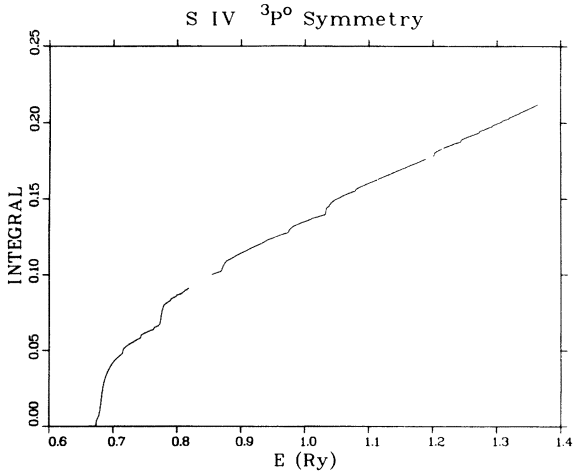

FIG. 5. Plot of the integral of Ω vs energy over the energy region 0.66–1.38 Ry for the $^3P^o$ symmetry.

TABLE IX. Total collision strengths for the $3s^2 3p\ ^2P$-$3s 3p^2\ ^4P$ transition in S IV.

E (Ry)	Ω (with resonances)	Ω (without resonances)
0.7	5.25	1.80
0.8	4.90	1.69
0.9	4.08	1.59
1.0	3.81	1.50
1.1	3.56	1.42
1.2	3.24	1.35
1.3	2.00	1.29

er, the total effect is to substantially change I and thus the rate coefficient from what it would have been if the resonance series had been absent.

In Table IX we give the total collision strength, with and without resonance enhancements included, summed over the eight symmetries considered here. The resonance-enhanced collision strength was calculated using the Gailitis average over one set of degenerate closed channels at a time. The nonresonance collision strengths were calculated with the distorted-wave approximation.[15] From the table one sees that the enhancement drops significantly every time a threshold in energy is crossed. This is due to the opening of channels that had been giving resonance enhancement to the $3s^2 3p(^2P)$-$3s\ 3p^2(^4P)$ transition.

In Table X we compare our resonance-enhanced collision strengths computed from the distorted-wave $\underline{R}$ matrix with those computed from Dufton and Kingston's $\underline{R}$ matrix above the resonance thresholds for the $^2P^o$-$^4P^e$ transition in S IV. The quantum-defect theory was used to obtain the collision strengths for the $^3P^e$ and $^3P^o$ symmetries at 0.70 Ry. We compare both the enhanced collision strength and the background collision strength. One sees that both the distorted-wave and close-coupling $\underline{R}$ matrices give nearly identical results. Thus, even though individual resonance widths may be in error by a factor of 2, the average resonance enhancement to the collision strength is predicted quite accurately.

Finally, we note that at 0.70 Ry our present method using the distorted-wave $\underline{R}$ matrix with a configuration interaction gives a total enhanced collision strength of 5.25 and a background collision strength of 1.8 for this transition in S IV. Thus, we find an enhancement of just under a factor of 3. At the same energy Dufton and Kingston appear to find an enhanced collision strength of slightly over 6 from their graph of $\overline{\Omega}$ vs temperature, their Fig. 4. Also, it appears that their background collision strength is slightly over 2, so that they also find a resonance enhancement of about a factor of 3. van

TABLE X. Comparison of Ω for the $^3P^e$ and $^3P^o$ symmetries for the $3s^2 3p\ ^2P$-$3s\ 3p^2\ ^4P$ transition in S IV at 0.70 Ry.

$\underline{R}$-matrix source	$\Omega\ ^3P^e$	$\Omega\ ^3P^o$
PCI[a]	0.52	0.55
DKRM[b]	0.55	0.55
PCI background	0.35	0.29
DKRM background	0.37	0.24

[a]PCI, Present calculations with configuration interaction included.
[b]DKRM, matrix from Dufton and Kingston (Ref. 4).

Wyngaarden and Henry[20] have made an estimate of this resonance enhancement by extrapolating collision strengths from the above threshold region to below threshold. They estimate an enhancement of approximately 2.1.

IV. CONCLUSION

We have used variations of the quantum-defect theory to compute collision strengths for selected transitions in O VI and S IV. We find that using distorted-wave matrix elements and ignoring coupling between different nondegenerate closed channels, we can accurately predict positions of resonances and can probably give the widths of strong resonances to better than a factor of 2. Moreover, we find that for the cases considered here, the resonance-enhanced collision strengths are given quite accurately compared to other methods, even when the enhancement is substantial. The method also applies if one uses close-coupling reactance matrix elements above the resonance thresholds and could be useful in locating resonances to be examined in detail by a close-coupling calculation. One of the advantages of this method is that the reactance matrix only needs to be calculated at a small number (five or six) of energy points in the above threshold energy region. The fit parameters are then used to calculate the matrix at all other energy points.

ACKNOWLEDGMENTS

The authors are grateful to Dr. R. Christensen for providing a copy of a preliminary version of RANAL. We also thank K. M. Aggarwal for sending us the close-coupling reactance matrix elements of Dufton and Kingston, and thank Dr. R. J. W. Henry for providing us his partial-wave collision strengths for O VI for comparison purposes prior to publication.

[1]L. P. Presnyakov and A. M. Urnov, J. Phys. B 8, 1280 (1975).
[2]Michael S. Pindzola, Phys. Rev. A 15, 2238 (1977).
[3]M. D. Hershkowitz and M. J. Seaton, J. Phys. B 6, 1176 (1973).
[4]P. L. Dufton and A. E. Kingston, J. Phys. B 13, 4277 (1980).
[5]D. Norcross and M. J. Seaton, J. Phys. B 3, 579 (1970).
[6]K. Bhadra and Ronald J. W. Henry, Phys. Rev. A 26, 1848 (1982).
[7]A. K. Pradhan, D. W. Norcross, and D. G. Hummer, Phys. Rev. A 23, 619 (1981).
[8]A. K. Pradhan, D. W. Norcross, and D. G. Hummer, Astrophys. J. 246, 1031 (1981).
[9]Robert D. Cowan, J. Phys. B 13, 1471 (1980).
[10]M. J. Seaton, J. Phys. B 2, 5 (1969).
[11]M. J. Seaton, Proc. Phys. Soc. London 88, 801 (1966).
[12]A. K. Pradhan and M. J. Seaton (unpublished).
[13]R. Christensen (private communication).
[14]M. Gailitis, Zh. Eksp. Teor. Fiz. 44, 1974 (1963) [Sov. Phys.—JETP 17, 1328 (1963)].
[15]James M. Peek and Joseph B. Mann, Phys. Rev. A 25, 749 (1982).
[16]L. A. Collins and B. I. Schneider, Phys. Rev. A 24, 2387 (1981).
[17]L. A. Collins and B. I. Schneider, Phys. Rev. A 27, 101 (1983).
[18]Robert D. Cowan, *Theory of Atomic Structure and Spectra* (University of California Press, Berkeley, 1981).
[19]K. M. Aggarwal (private communication).
[20]W. L. van Wyngaarden and Ronald J. W. Henry, Astrophys. J. 246, 1040 (1981).